Update on the indication of a composition anisotropy above $10^{18.7}$ eV in the hybrid data of the Pierre Auger Observatory

Eric Mayotte* [a,b] and Thomas Fitoussi[c] for the Pierre Auger Collaboration[d]
* Speaker: emayotte@mines.edu

[a] Colorado School of Mines, Department of Physics, Golden CO, USA
[b] Bergische Universität Wuppertal, Department of Physics, Wuppertal, Germany
[c] Karlsruhe Institute of Technology, Institute for Astroparticle Physics, Karlsruhe, Germany
[d] Observatorio Pierre Auger, Malargüe, Argentina

6th International Symposium on Ultra High Energy Cosmic Rays
UHECR 2022
L'Aquila, Italy October 3 - 7 2022

PIERRE AUGER OBSERVATORY

A rather simplified summary of motivation

- **Primary UHECR composition generally appears to be mixed in nature and gets heavier with increasing energy.**
  → CR primaries arriving with the same energy have different rigidities.
- The UHECR flux is definitely anisotropic above 8 EeV
  → Magnetic fields will distort injection anisotropies differently for each mass component.
- The strongest magnetic field affecting locally observed flux is the GMF.
  → Distortion effects strongest for trajectories near to the galactic plane, weakest away from it.
- Possible effects admittedly highly complex and dependent on coherent/turbulent B-field strengths, primary composition profile, and external source distribution;

→ however, possibility exists for anisotropy which depends on composition which correlates GMF and therefore the Galactic plane.

A rather simplified summary of motivation

- Primary UHECR composition generally appears to be mixed in nature and gets heavier with increasing energy.
  → CR primaries arriving with the same energy have different rigidities.
- **The UHECR flux is definitely anisotropic above 8 EeV**
  → Magnetic fields will distort injection anisotropies differently for each mass component.
- The strongest magnetic field affecting locally observed flux is the GMF.
  → Distortion effects strongest for trajectories near to the galactic plane, weakest away from it.
- Possible effects admittedly highly complex and dependent on coherent/turbulent B-field strengths, primary composition profile, and external source distribution;

→ however, possibility exists for anisotropy which depends on composition which correlates GMF and therefore the Galactic plane.

A rather simplified summary of motivation

- Primary UHECR composition generally appears to be mixed in nature and gets heavier with increasing energy.
  → CR primaries arriving with the same energy have different rigidities.
- The UHECR flux is definitely anisotropic above 8 EeV
  → Magnetic fields will distort injection anisotropies differently for each mass component.
- **The strongest magnetic field affecting locally observed flux is the GMF.**
  → Distortion effects strongest for trajectories near to the galactic plane, weakest away from it.
- Possible effects admittedly highly complex and dependent on coherent/turbulent B-field strengths, primary composition profile, and external source distribution;

→ however, possibility exists for anisotropy which depends on composition which correlates GMF and therefore the Galactic plane.

A rather simplified summary of motivation

- Primary UHECR composition generally appears to be mixed in nature and gets heavier with increasing energy.
  $\rightarrow$ CR primaries arriving with the same energy have different rigidities.
- The UHECR flux is definitely anisotropic above 8 EeV
  $\rightarrow$ Magnetic fields will distort injection anisotropies differently for each mass component.
- The strongest magnetic field affecting locally observed flux is the GMF.
  $\rightarrow$ Distortion effects strongest for trajectories near to the galactic plane, weakest away from it.
- **Possible effects admittedly highly complex and dependent on coherent/turbulent B-field strengths, primary composition profile, and external source distribution;**

$\rightarrow$ however, possibility exists for anisotropy which depends on composition which correlates GMF and therefore the Galactic plane.

A rather simplified summary of motivation

- Primary UHECR composition generally appears to be mixed in nature and gets heavier with increasing energy.
  $\rightarrow$ CR primaries arriving with the same energy have different rigidities.
- The UHECR flux is definitely anisotropic above 8 EeV
  $\rightarrow$ Magnetic fields will distort injection anisotropies differently for each mass component.
- The strongest magnetic field affecting locally observed flux is the GMF.
  $\rightarrow$ Distortion effects strongest for trajectories near to the galactic plane, weakest away from it.
- Possible effects admittedly highly complex and dependent on coherent/turbulent B-field strengths, primary composition profile, and external source distribution;

$\rightarrow$ **however, possibility exists for anisotropy which depends on composition which correlates GMF and therefore the Galactic plane.**

How to test? Measure UHECR mass on and off plane

1. **Use the composition sensitivity of the atmospheric depth of shower maximum, X_{max}, to test!**
   → Measured via the hybrid method outlined in (A. Aab et al. 2014) and (Yushkov 2020)
2. Define the on- and off-plane regions using some Galactic latitude splitting angle b_{split}

   On-plane: $|b_i| \leq b_{split}$ Off-plane: $|b_i| > b_{split}$

3. Obtain a Test Statistic comparing the on- and off-plane X_{max} distributions using the Anderson-Darling 2-Sample test (Anderson and Darling 1952)
4. Perform a scan over roughly 50 % of the data to select E_{min} and b_{split} prescription.
5. Apply the scan selected thresholds as a prescription to remaining data
6. Calculate statistical significance using Monte-Carlo and random skies
7. Evaluate systematic uncertainties and their effects on result significance

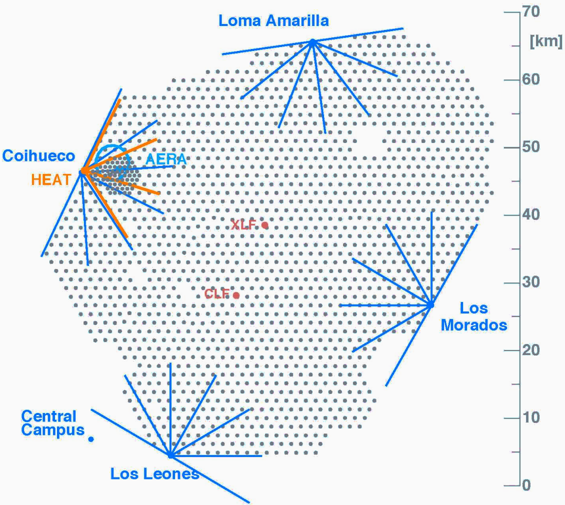

The Observatory (Aab et al. 2015)

- FD: 27 fluorescence telescopes
- SD: 1660 water-Cherenkov detectors
- Hybrid measurement concept:
  - → Core timing/location with SD
  - → Geometry with FD pixel trace
  - → Energy and X_{max} from FD light profile

Event X_{max} values obtained using:

the reconstruction, selection, and methods from (Yushkov 2020) on hybrid data collected between 01.12.2004–31.12.2018

- see backup for details -

Step-by-step testing method

1. Use the composition sensitivity of the atmospheric depth of shower maximum, X_{max}, to test!
   → Measured via the hybrid method outlined in (A. Aab et al. 2014) and (Yushkov 2020)

2. **Define the on- and off-plane regions using some Galactic latitude splitting angle b_{split}**

   On-plane: $|\ b_i\ | \leq b_{\mathrm{split}}$ **Off-plane:** $|\ b_i\ | > b_{\mathrm{split}}$

3. Obtain a Test Statistic comparing the on- and off-plane X_{max} distributions using the Anderson-Darling 2-Sample test (Anderson and Darling 1952)

4. Perform a scan over roughly 50 % of the data to select E_{min} and b_{split} prescription.

5. Apply the scan selected thresholds as a prescription to remaining data

6. Calculate statistical significance using Monte-Carlo and random skies

7. Evaluate systematic uncertainties and their effects on result significance

Step-by-step testing method

1. Use the composition sensitivity of the atmospheric depth of shower maximum, X_{max}, to test!
   → Measured via the hybrid method outlined in (A. Aab et al. 2014) and (Yushkov 2020)
2. Define the on- and off-plane regions using some Galactic latitude splitting angle b_{split}

   On-plane: $|\ b_i\ | \leq b_{\mathrm{split}}$ Off-plane: $|\ b_i\ | > b_{\mathrm{split}}$

3. **Obtain a Test Statistic comparing the on- and off-plane X_{max} distributions using the Anderson-Darling 2-Sample test (Anderson and Darling 1952)**
4. Perform a scan over roughly 50 % of the data to select E_{min} and b_{split} prescription.
5. Apply the scan selected thresholds as a prescription to remaining data
7. Calculate statistical significance using Monte-Carlo and random skies
8. Evaluate systematic uncertainties and their effects on result significance

Step-by-step testing method

1. Use the composition sensitivity of the atmospheric depth of shower maximum, X_{max}, to test!
   $\rightarrow$ Measured via the hybrid method outlined in (A. Aab et al. 2014) and (Yushkov 2020)
2. Define the on- and off-plane regions using some Galactic latitude splitting angle b_{split}

   $$\text{On-plane: } |\, b_i \,| \leq b_{\text{split}} \qquad \text{Off-plane: } |\, b_i \,| > b_{\text{split}}$$

3. Obtain a Test Statistic comparing the on- and off-plane X_{max} distributions using the Anderson-Darling 2-Sample test (Anderson and Darling 1952)
4. **Perform a scan over roughly 50 % of the data to select E_{min} and b_{split} prescription**.
5. Apply the scan selected thresholds as a prescription to remaining data
6. Calculate statistical significance using Monte-Carlo and random skies
7. Evaluate systematic uncertainties and their effects on result significance

Data scan and prescription

Data-driven selection of energy and latitude thresholds

- Scan over roughly the first 50 % of data taken
- 5° steps in b and $0.1\,\lg(E/\mathrm{eV})$ steps in energy
- **Highest TS of 8.35 for:** $\rightarrow E_{\mathrm{min}} = 10^{18.7}\,\mathrm{eV}$
  $\rightarrow b_{\mathrm{split}} = 30^\circ$

Set as prescription for remaining data

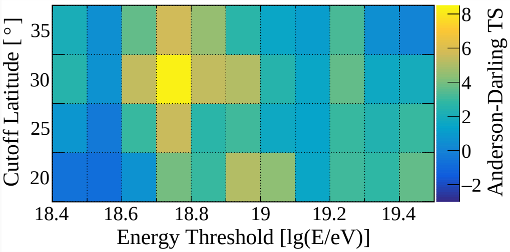

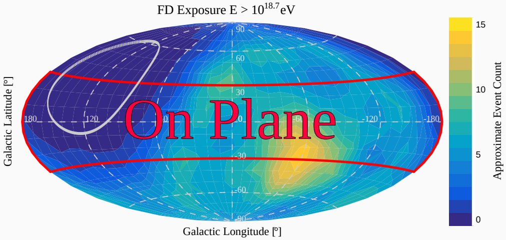

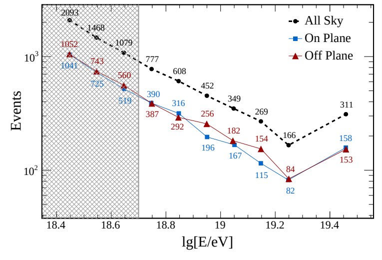

Step-by-step testing method

1. Use the composition sensitivity of the atmospheric depth of shower maximum, X_{max}, to test!
   $\rightarrow$ Measured via the hybrid method outlined in (A. Aab et al. 2014) and (Yushkov 2020)

2. Remove the X_{max} elongation rate so events over a threshold energy, E_{min}, can be combined

3. Define the on- and off-plane regions using some Galactic latitude splitting angle b_{split}

$$\text{On-plane: } |\ b_i\ | \leq b_{\text{split}} \qquad \text{Off-plane: } |\ b_i\ | > b_{\text{split}}$$

4. Obtain a Test Statistic comparing the on- and off-plane X_{max} distributions using the Anderson-Darling 2-Sample test (Anderson and Darling 1952)

5. Perform a scan over roughly 50 % of the data to select E_{min} and b_{split} prescription.

6. **Apply the scan selected thresholds as a prescription to remaining data**

7. Calculate statistical significance using Monte-Carlo and random skies

8. Evaluate systematic uncertainties and their effects on result significance

Composition Plots

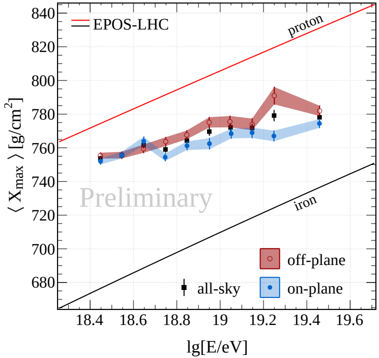

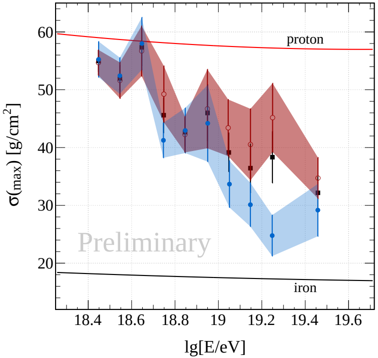

Good separation for above $10^{18.7}$ eV

Indicates a heavier mean mass on-plane for all energies above the ankle

Composition Plots

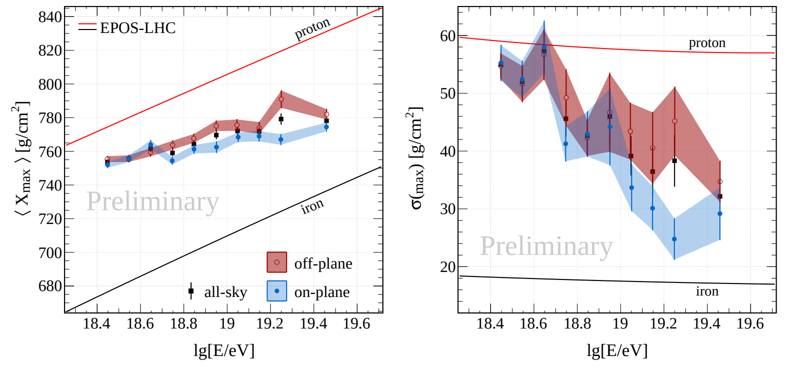

Good separation for above $10^{18.7}$ eV

Indicates a heavier mean mass on-plane for all energies above the ankle

On- and off-plane X_{max} difference in remaining data

Unscanned data: $TS = 12.6$

$$\boldsymbol{\Delta\langle X'_{max}\rangle = 10.5 \pm 2.5^{+2.1}_{-2.2}}\ \mathrm{g/cm^2}$$

$$\boldsymbol{\Delta\sigma(X'_{max}) = 5.9 \pm 3.1^{+3.5}_{-2.5}}\ \mathrm{g/cm^2}$$

All data: $TS = 21.0$

$$\boldsymbol{\Delta\langle X'_{max}\rangle = 9.1 \pm 1.6^{+2.1}_{-2.2}}\ \mathrm{g/cm^2}$$

$$\boldsymbol{\Delta\sigma(X'_{max}) = 5.9 \pm 2.1^{+3.5}_{-2.5}}\ \mathrm{g/cm^2}$$

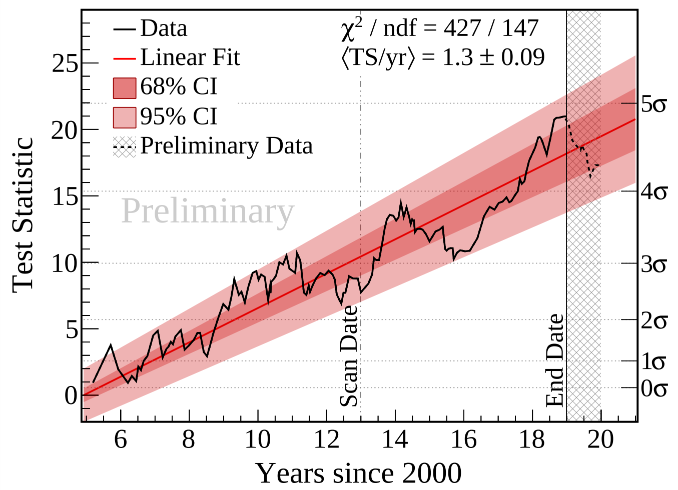

Step-by-step testing method

1. Use the composition sensitivity of the atmospheric depth of shower maximum, $X_{\max}$, to test!
   → Measured via the hybrid method outlined in (A. Aab et al. 2014) and (Yushkov 2020)
2. Remove the $X_{\max}$ elongation rate so events over a threshold energy, $E_{\min}$, can be combined
3. Define the on- and off-plane regions using some Galactic latitude splitting angle b_{split}

   $$\text{On-plane: } |\, b_i \,| \leq b_{\text{split}} \qquad \text{Off-plane: } |\, b_i \,| > b_{\text{split}}$$

4. Obtain a Test Statistic comparing the on- and off-plane $X_{\max}$ distributions using the Anderson-Darling 2-Sample test (Anderson and Darling 1952)
5. Perform a scan over roughly 50 % of the data to select $E_{\min}$ and b_{split} prescription.
6. Apply the scan selected thresholds as a prescription to remaining data
7. **Calculate statistical significance using Monte-Carlo and random skies**
8. Evaluate systematic uncertainties and their effects on result significance

Statistical significance is calculated by duplicating the analysis on many random skies

- The data is shuffled in arrival direction to form random skies for each MC trial from which TS are extracted
- Scan duplicated in evaluation of the scanned + unscanned dataset
  → Imposes heavy penalization (only 0.5 σ gained)

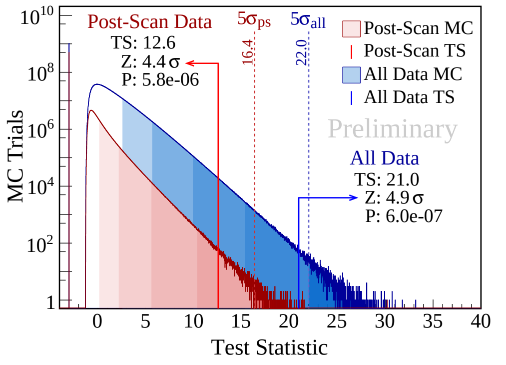

Blinded data:
Post-penalization 4.4 σ Stat.
Chance probability 1 in 172,000

All available data:
Post-penalization 4.9 σ Stat.
Chance probability 1 in 1,678,000

Step-by-step testing method

1. Use the composition sensitivity of the atmospheric depth of shower maximum, $X_{\max}$, to test!
   → Measured via the hybrid method outlined in (A. Aab et al. 2014) and (Yushkov 2020)
2. Remove the $X_{\max}$ elongation rate so events over a threshold energy, $E_{\min}$, can be combined
3. Define the on- and off-plane regions using some Galactic latitude splitting angle b_{split}

   $$\text{On-plane: } |\ b_i\ | \leq b_{\text{split}} \qquad \text{Off-plane: } |\ b_i\ | > b_{\text{split}}$$

4. Obtain a Test Statistic comparing the on- and off-plane $X_{\max}$ distributions using the Anderson-Darling 2-Sample test (Anderson and Darling 1952)
5. Perform a scan over roughly 50 % of the data to select $E_{\min}$ and b_{split} prescription.
6. Apply the scan selected thresholds as a prescription to remaining data
7. Calculate statistical significance using Monte-Carlo and random skies
8. **Evaluate systematic uncertainties and their effects on result significance**

Sources of systematic uncertainty

Systematic effects which apply equally to both regions will cancel in a comparison between them

- Local event arrival geometries, camera signatures and atmospheric conditions very similar
- Same detectors, reconstruction method and analysis technique for both regions

Non-canceling systematic uncertainty:

$^{+2.10}_{-2.23}$ g/cm^2 for $\Delta\langle X'_{max}\rangle$ (Off-On)

$^{+3.49}_{-2.48}$ g/cm^2 for $\Delta\sigma(X'_{max})$ (Off-On)

Details in backup

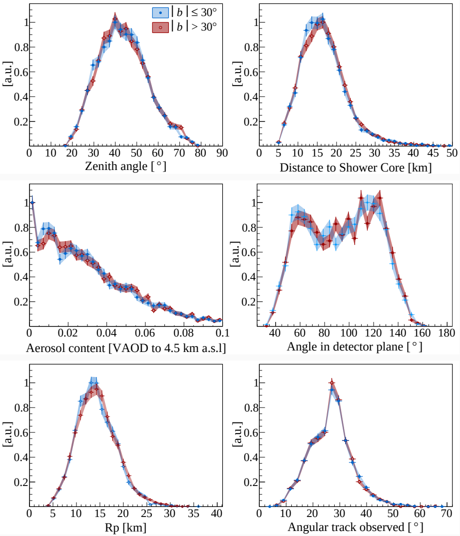

Observed differences much larger than systematics

- Observed $\Delta\langle X'_{\max}\rangle$(Off-On) is 4.1 times larger than its systematic uncertainty
- Observed $\Delta\sigma\,(X'_{\max})$(Off-On) is 2.4 times larger than its systematic uncertainty

Check for possibility of systematics increasing probability for a large fluctuation:

- Probability estimated by shifting random skies by the systematic uncertainty to increase occurrence rate of extreme results

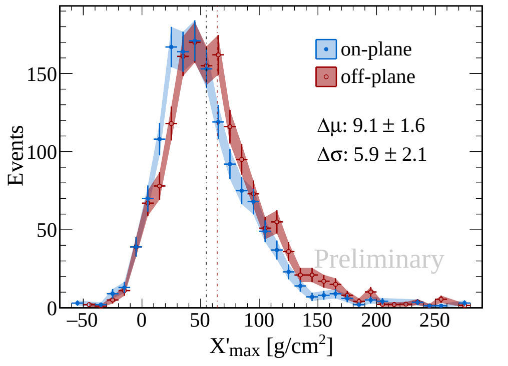

At least 3.3 σ with systematic effects taken as the resultant confidence level.

Observed differences much larger than systematics

- Observed $\Delta\langle X'_{\text{max}}\rangle$(Off-On) is 4.1 times larger than its systematic uncertainty
- Observed $\Delta\sigma\,(X'_{\text{max}})$(Off-On) is 2.4 times larger than its systematic uncertainty

Check for possibility of systematics increasing probability for a large fluctuation:

- Probability estimated by shifting random skies by the systematic uncertainty to increase occurrence rate of extreme results

At least 3.3 σ with systematic effects taken as the resultant confidence level.

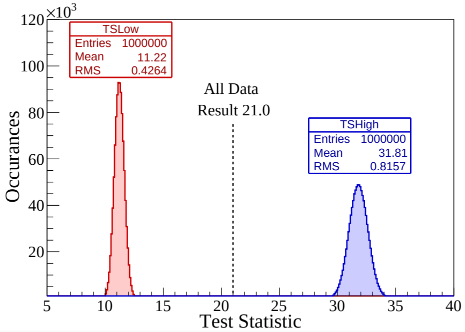

Cross checks: results by FD Site and Zenith angle

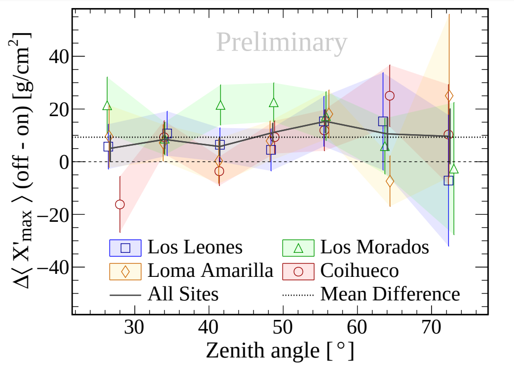

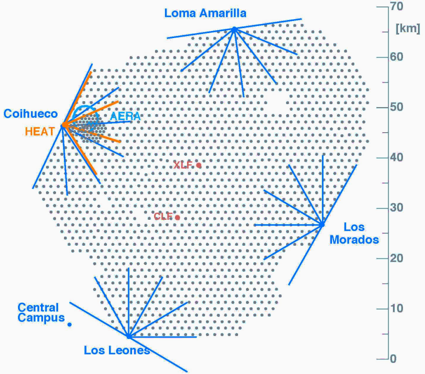

On/Off difference independently seen in all FD sites and 22/28 zenith bins

Because each FD site FoV differs by 90°
Systematic causes can not
easily explain the on/off difference.

Cross checks: results by FD Site and Zenith angle

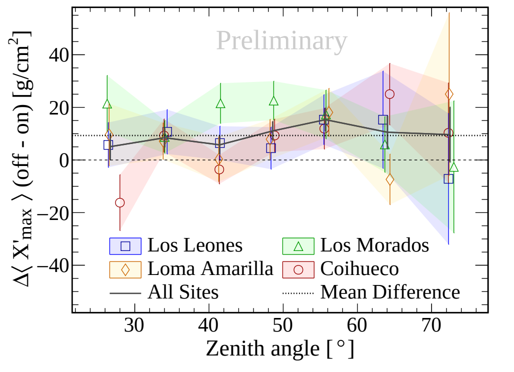

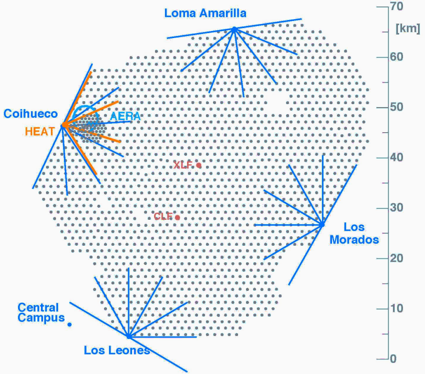

On/Off difference independently seen in all FD sites and 22/28 zenith bins

Because each FD site FoV differs by 90°
Systematic causes can not
easily explain the on/off difference.

Independent test result on new data needed

- AugerPrime promises to deliver sensitivity and statistics to solidify or clarify nature of FD signal
- SD-only DNN may meet required sensitivity, and is under review for event-by-event anisotropy studies

⇒ FD data that was cut from highest-quality $X_{\max}$ analysis immediately available

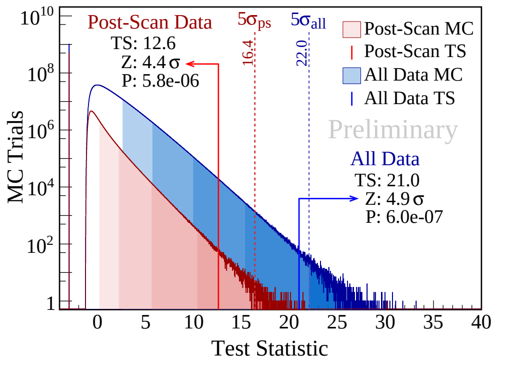

Solution: use opposite selection of FidFoV cut, out-FidFoV, to form an independent data sample

- Individual events satisfy all quality cuts on measurement and reconstruction quality → are well suited to the test

⇒ $X_{\max}$ acceptance in out-FidFoV is not flat over range of observed events → needs to be considered

Rather surprising result at only 3.3 σ with systematics

Independent cross-check on unused FD data

Independent test result on new data needed

- AugerPrime promises to deliver sensitivity and statistics to solidify or clarify nature of FD signal
- SD-only DNN may meet required sensitivity, and is under review for event-by-event anisotropy studies

⇒ **FD data that was cut from highest-quality X_{max} analysis immediately available**

Solution: use opposite selection of FidFoV cut, out-FidFoV, to form an independent data sample

- Individual events satisfy all quality cuts on measurement and reconstruction quality → are well suited to the test

⇒ X_{max} acceptance in out-FidFoV is not flat over range of observed events → needs to be considered

Table 1: Quality Selection

Cut name	N	Eff [%]
Raw events	1.24e+7	–
Data quality	2646577	21.3
Atmospheric Quality	1687395	63.8
Reconstruction/trigger quality	426729	25.3
Energy greater than $10^{18.4}$ eV	25546	6.0
Profile reconstruction quality	14664	57.4
Fiducial field-of-view (FidFoV)	8017	54.6

In the out-FidFoV data 45.4 % of high quality events are available for test

Independent cross-check on unused FD data

Independent test result on new data needed

- AugerPrime promises to deliver sensitivity and statistics to solidify or clarify nature of FD signal
- SD-only DNN may meet required sensitivity, and is under review for event-by-event anisotropy studies

⇒ FD data that was cut from highest-quality X_{max} analysis immediately available

Solution: use opposite selection of FidFoV cut, out-FidFoV, to form an independent data sample

- Individual events satisfy all quality cuts on measurement and reconstruction quality → are well suited to the test

⇒ X_{max} acceptance in out-FidFoV is not flat over range of observed events → needs to be considered

Table 1: Quality Selection

Cut name	N	Eff [%]
Raw events	1.24e+7	–
Data quality	2646577	21.3
Atmospheric Quality	1687395	63.8
Reconstruction/trigger quality	426729	25.3
Energy greater than $10^{18.4}$ eV	25546	6.0
Profile reconstruction quality	14664	57.4
Fiducial field-of-view (FidFoV)	**8017**	**54.6**

In the out-FidFoV data 45.4 % of high quality events are available for test

On/Off analysis of out-FidFoV dataset

- Out-FidFoV shows a $\Delta\langle X_{\mathrm{max}}\rangle$ of $\sim 5\,\mathrm{g/cm^2}$
- Anderson-Darling test rejects uniform composition at $2.2\,\sigma$

⇒ Question: is lower result in tension with main result, or due to decreased sensitivity of out-FidFoV data?

Evaluating the effects of out-FidFoV acceptance/resolution

1. Generate many mock datasets based on a $\Delta\langle X_{\mathrm{max}}\rangle$ of $9.1\,\mathrm{g/cm^2}$ and $\Delta\sigma\,(X_{\mathrm{max}})$ of $5.9\,\mathrm{g/cm^2}$
2. Forward fold the non-flat X_{max} acceptance and lower resolution of the out-FidFoV dataset onto the mocks
3. Test resulting distributions with AD test and compare with out-FidFoV result

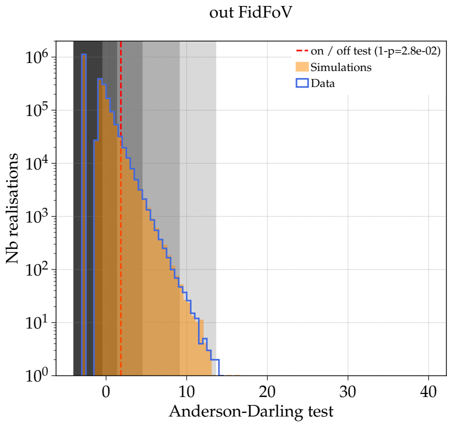

On/Off analysis of out-FidFoV dataset

- Out-FidFoV shows a $\Delta\langle X_{\rm max}\rangle$ of $\sim 5\,{\rm g/cm^2}$
- Anderson-Darling test rejects uniform composition at $2.2\,\sigma$

⇒ Question: is lower result in tension with main result, or due to decreased sensitivity of out-FidFoV data?

Evaluating the effects of out-FidFoV acceptance/resolution

1. Generate many mock datasets based on a $\Delta\langle X_{\rm max}\rangle$ of $9.1\,{\rm g/cm^2}$ and $\Delta\sigma\,(X_{\rm max})$ of $5.9\,{\rm g/cm^2}$
2. Forward fold the non-flat $X_{\rm max}$ acceptance and lower resolution of the out-FidFoV dataset onto the mocks
3. Test resulting distributions with AD test and compare with out-FidFoV result

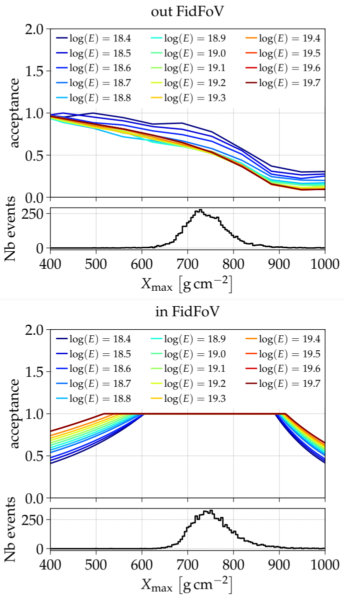

Independent cross-check on unused FD data

On/Off analysis of out-FidFoV dataset

- Out-FidFoV shows a $\Delta\langle X_{\max}\rangle$ of $\sim 5\,\mathrm{g/cm^2}$
- Anderson-Darling test rejects uniform composition at $2.2\,\sigma$

$\Rightarrow$ Question: is lower result in tension with main result, or due to decreased sensitivity of out-FidFoV data?

Evaluating the effects of out-FidFoV acceptance/resolution

1. Generate many mock datasets based on a $\Delta\langle X_{\max}\rangle$ of $9.1\,\mathrm{g/cm^2}$ and $\Delta\sigma\left(X_{\max}\right)$ of $5.9\,\mathrm{g/cm^2}$
2. Forward fold the non-flat $X_{\max}$ acceptance and lower resolution of the out-FidFoV dataset onto the mocks
3. **Test resulting distributions with AD test and compare with out-FidFoV result**

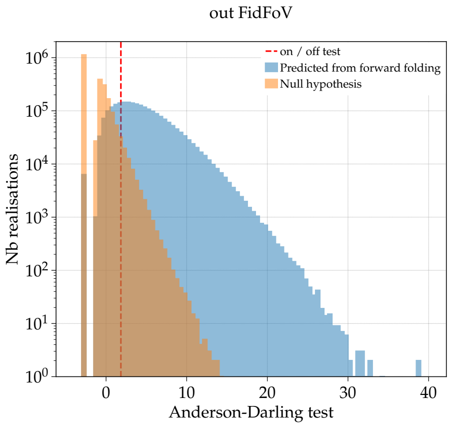

out-FidFoV Result near peak

$\sim$38 % of tests have lower TS

Lends support to main result

Map compares $\langle X_{max} \rangle$ of events within 30° of each bin to the rest of the sky

Red: lower mass than rest of sky
Blue: higher mass than rest of sky

- TS is Welch's T-Test applied to in- and out-of-hat X'_{max} distribution
- Detector/analysis effects corrected for by event arrival declination

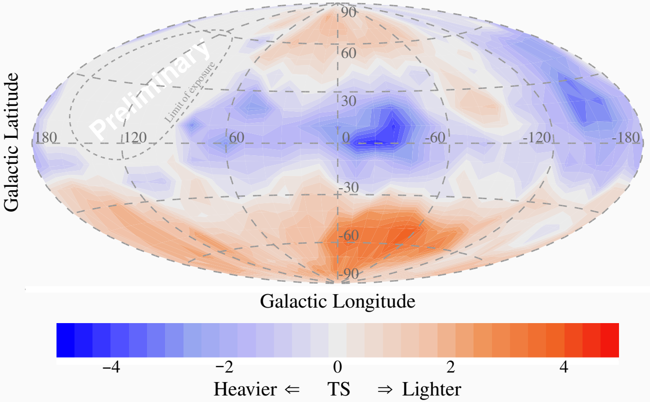

Discussion

- **Verifies mixed composition above the ankle.**
- Suggests GMF could cause composition anisotropies; however...
- An unrelated anisotropy may have instead been captured by serendipitous use of the Galactic plane as a catalog:

  → Mass-dependent propagation effects can create composition anisotropies (N. Globus et al. 2008; Ding, Globus, and Farrar. 2021)

  → However magnitude of difference is in significant tension with current models (Allard et al. 2021)
- Due to impending changes to our X_{max} reconstruction and atmospheric corrections, results are preliminary

  → New FD X_{max} publication in preparation

  → This result will be fully published in parallel

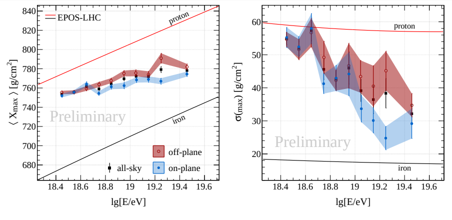

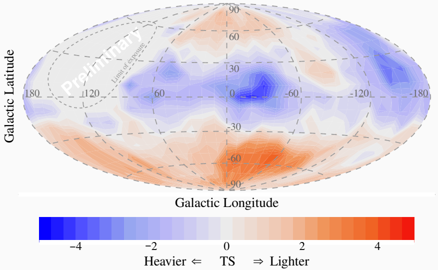

- Verifies mixed composition above the ankle.
- **Suggests GMF could cause composition anisotropies; however...**
- An unrelated anisotropy may have instead been captured by serendipitous use of the Galactic plane as a catalog:

  → Mass-dependent propagation effects can create composition anisotropies (N. Globus et al. 2008; Ding, Globus, and Farrar. 2021)

  → However magnitude of difference is in significant tension with current models (Allard et al. 2021)

- Due to impending changes to our X_{max} reconstruction and atmospheric corrections, results are preliminary

  → New FD X_{max} publication in preparation

  → This result will be fully published in parallel

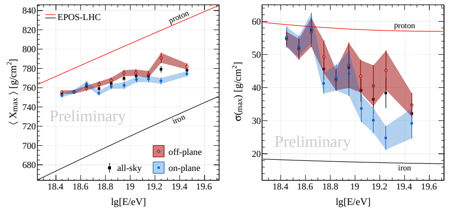

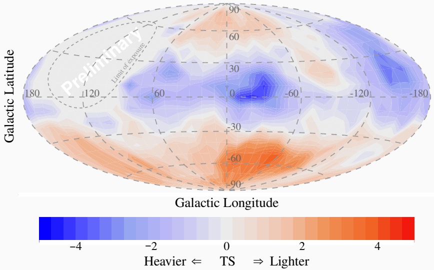

Discussion

- Verifies mixed composition above the ankle.
- Suggests GMF could cause composition anisotropies; however...
- **An unrelated anisotropy may have instead been captured by serendipitous use of the Galactic plane as a catalog:**

  → Mass-dependent propagation effects can create composition anisotropies (N. Globus et al. 2008; Ding, Globus, and Farrar. 2021)

  → However magnitude of difference is in significant tension with current models (Allard et al. 2021)

- Due to impending changes to our X_{max} reconstruction and atmospheric corrections, results are preliminary

  → New FD X_{max} publication in preparation

  → This result will be fully published in parallel

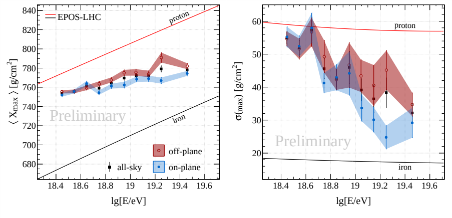

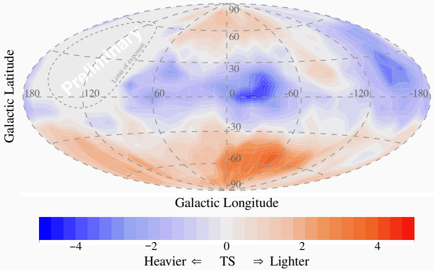

Discussion

- Verifies mixed composition above the ankle.
- Suggests GMF could cause composition anisotropies; however...
- An unrelated anisotropy may have instead been captured by serendipitous use of the Galactic plane as a catalog:

  → Mass-dependent propagation effects can create composition anisotropies (N. Globus et al. 2008; Ding, Globus, and Farrar. 2021)

  → However magnitude of difference is in significant tension with current models (Allard et al. 2021)

- **Due to impending changes to our X_{max} reconstruction and atmospheric corrections, results are preliminary**

  → New FD X_{max} publication in preparation

  → This result will be fully published in parallel

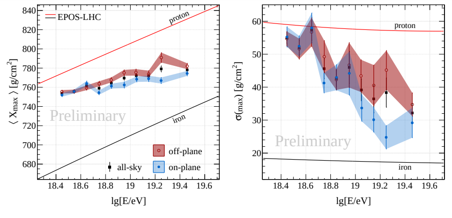

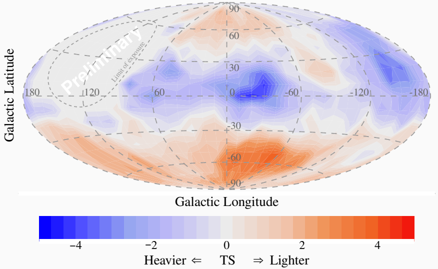

References

Aab et al. (2015). "The Pierre Auger Cosmic Ray Observatory". In: Nucl. Instrum. Meth. A 798, pp. 172–213. DOI: 10.1016/j.nima.2015.06.058. arXiv: 1502.01323 [astro-ph.IM].

Aab, Alexander et al. (2014). "Depth of Maximum of Air-Shower Profiles at the Pierre Auger Observatory: Measurements at Energies above $10^{17.8}$ eV". In: PRD 90.12, p. 122005. DOI: 10.1103/PhysRevD.90.122005.

Allard, D. et al. (Oct. 2021). "What can be learnt from UHECR anisotropies observations? Paper I : large-scale anisotropies and composition features". In: arXiv: 2110.10761 [astro-ph.HE].

Anderson, T. W. and D. A. Darling (1952). "Asymptotic Theory of Certain "Goodness of Fit" Criteria Based on Stochastic Processes". In: Ann. Math. Statist. 23.2, pp. 193–212. DOI: 10.1214/aoms/1177729437. URL: https://doi.org/10.1214/aoms/1177729437.

Bellido, Jose (2018). "Depth of maximum of air-shower profiles at the Pierre Auger Observatory". In: PoS ICRC2017. Ed. by Darko Veberic, p. 506. DOI: 10.22323/1.301.0506.

Ding, Globus, and Farrar. (2021). "The Imprint of Large Scale Structure on the Ultra-High-Energy Cosmic Ray Sky". In: Astrophys. J. Lett. 913.1, p. L13. DOI: 10.3847/2041-8213/abf11e. arXiv: 2101.04564 [astro-ph.HE].

Erdmann, Martin et al. (2016). "The Nuclear Window to the Extragalactic Universe". In: Astropart. Phys. 85, pp. 54–64. DOI: 10.1016/j.astropartphys.2016.10.002.

Farrar (2014). "The Galactic magnetic field and ultrahigh-energy cosmic ray deflections". In: C R Phys 15.4, pp. 339–348.

Farrar and Sutherland (2019). "Deflections of UHECRs in the Galactic magnetic field". In: JCAP 05, p. 004. DOI: 10.1088/1475-7516/2019/05/004.

Globus, N. et al. (2008). "Propagation of high-energy cosmic rays in extragalactic turbulent magnetic fields: resulting energy spectrum and composition". In: Astron. Astrophys. 479, p. 97. DOI: 10.1051/0004-6361:20078653.

Jansson, Ronnie and Glennys R. Farrar (2012). "A New Model of the Galactic Magnetic Field". In: ApJ. 757, p. 14. DOI: 10.1088/0004-637X/757/1/14.

Pshirkov, M. et al. (2011). "Deriving global structure of the Galactic Magnetic Field from Faraday Rotation Measures of extragalactic sources". In: Astrophys. J. 738, p. 192. DOI: 10.1088/0004-637X/738/2/192.

Mass Composition of Cosmic Rays with Energies above $10^{17.2}$ eV from the Hybrid Data of the Pierre Auger Observatory (2020). Vol. ICRC2019, p. 482. DOI: 10.22323/1.358.0482.

Potential effects of the GMF on a mixed UHECR flux

- (Erdmann et al. 2016) showed definite transition from diffusive to ballistic propagation in GMF around 6 EV
- (Farrar and Sutherland 2019) showed GMF obscures sources and lenses their images off the plane
- (Farrar 2014) showed effect where images of off-plane sources are lensed toward the plane
- Effect depends on primary rigidity:
  - → no effect particles with $R < 6$ EV
  - → deflection starts around $R = 6$ EV
  - → weakens for higher rigidity particles
- UHECR composition mixed, therefore as energy climbs:
  - → effect starts then weakens for lightest primaries
  - → kicks in for progressively heavier components bringing them to the plane as UHECR point to sources

(Farrar and Sutherland 2019)

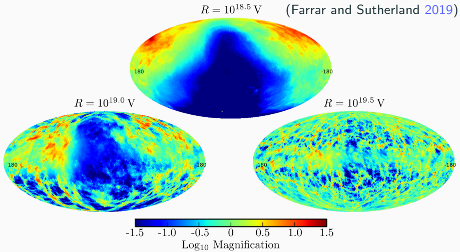

Relative magnification based on source position

(Farrar 2014)

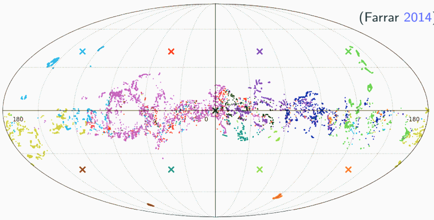

Lensing of off-plane sources – proton 10 EeV

Composition Sky Map - RA/Dec

Map compares $\langle X_{\max} \rangle$ of events within 30° of each bin to the rest of the sky

Red: lower mass than rest of sky
Blue: higher mass than rest of sky

- TS is Welch's T-Test applied to in- and out-of-hat $X'_{\max}$ distribution
- Detector/analysis effects corrected for by event arrival declination

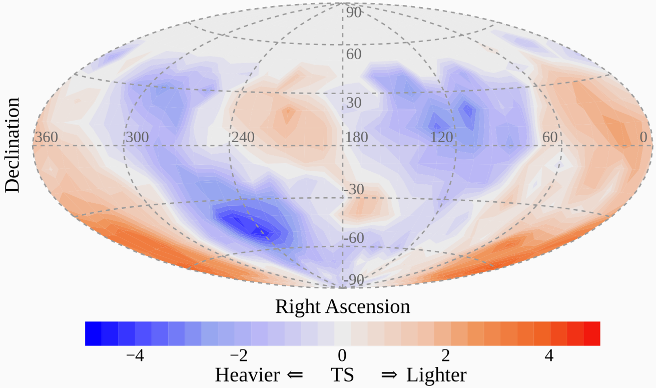

Removal of X_{max} elongation rate

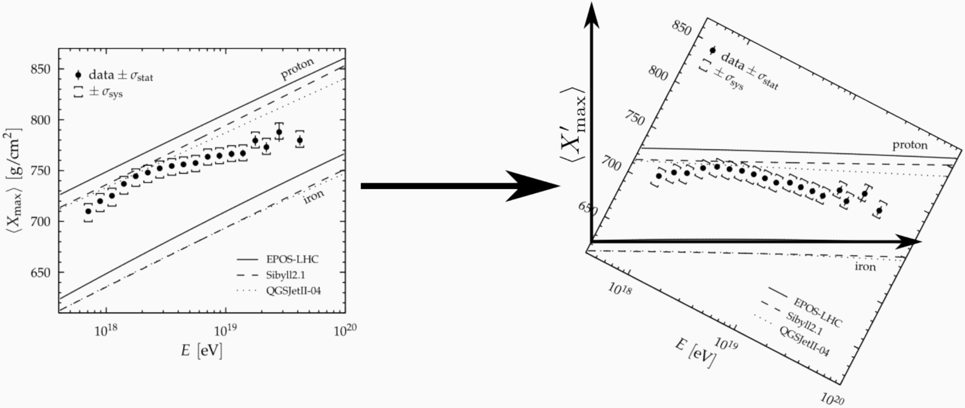

$$X'_{max} = X_{max} - \underbrace{\left(649 + 63.1 \log_{10}\left(E_{rec}/\,\text{EeV}\right) + 1.97 \log_{10}\left(E_{rec}/\,\text{EeV}\right)^2\right)}_{\text{EPOS-LHC elongation rate for iron}}$$

Choice of hadronic model has insignificant influence on end result ($\approx 0.02\,\text{g/cm}^2$)

- **(Erdmann et al. 2016) showed transition from diffusive to ballistic propagation in the GMF around 4 - 6 EV using both JF12 (Jansson and G. R. Farrar 2012) and PTK11 (Pshirkov et al. 2011)**
- Threshold dependence on Galactic latitude of CR
- At fixed energy above this limit:
  High mass → diffusive → isotropic arrival
  Low mass → ballistic → preserve some source anisotropy
- Differing horizon of each primary species introduces potential of differing source distributions (N. Globus et al. 2008)

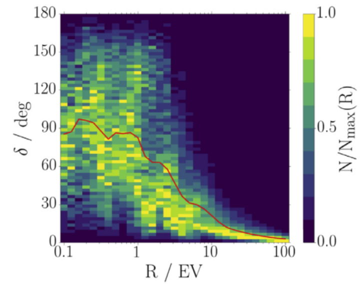

(Erdmann et al. 2016)

Motivating mass dependent anisotropies

- (Erdmann et al. 2016) showed transition from diffusive to ballistic propagation in the GMF around 4 - 6 EV using both JF12 (Jansson and G. R. Farrar 2012) and PTK11 (Pshirkov et al. 2011)
- **Threshold dependence on Galactic latitude of CR**
- At fixed energy above this limit:
  High mass → diffusive → isotropic arrival
  Low mass → ballistic → preserve some source anisotropy
- Differing horizon of each primary species introduces potential of differing source distributions (N. Globus et al. 2008)

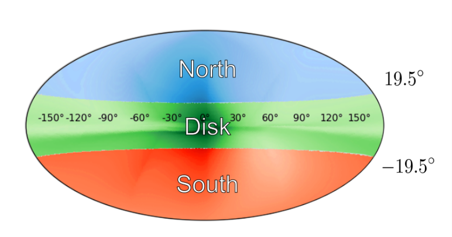

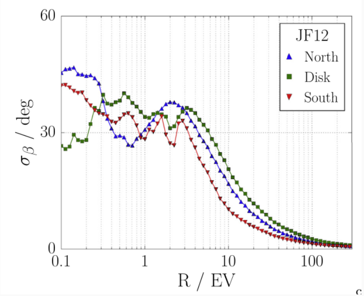

(Erdmann et al. 2016)

- (Erdmann et al. 2016) showed transition from diffusive to ballistic propagation in the GMF around 4 - 6 EV using both JF12 (Jansson and G. R. Farrar 2012) and PTK11 (Pshirkov et al. 2011)
- Threshold dependence on Galactic latitude of CR
- **At fixed energy above this limit:**
  High mass → diffusive → isotropic arrival
  Low mass → ballistic → preserve some source anisotropy
- Differing horizon of each primary species introduces potential of differing source distributions (N. Globus et al. 2008)

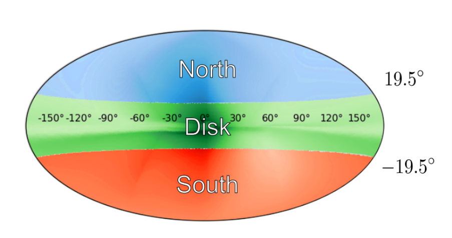

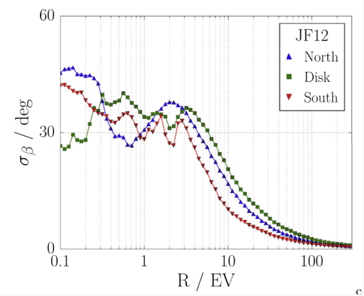

(Erdmann et al. 2016)

Motivating mass dependent anisotropies

- (Erdmann et al. 2016) showed transition from diffusive to ballistic propagation in the GMF around 4 - 6 EV using both JF12 (Jansson and G. R. Farrar 2012) and PTK11 (Pshirkov et al. 2011)

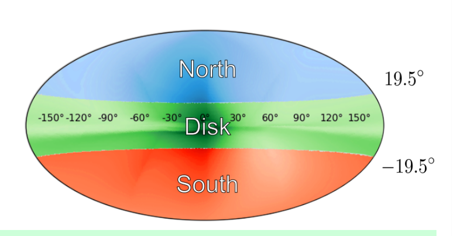

These give rise to the possibility of mass dependent anisotropies in the UHECR flux associated with GMF.

High mass → diffusive → isotropic arrival
Low mass → ballistic → preserve some source anisotropy

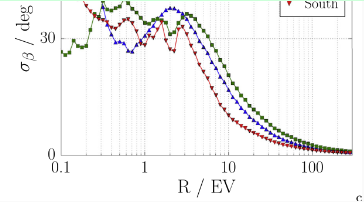

- **Differing horizon of each primary species introduces potential of differing source distributions (N. Globus et al. 2008)**

(Erdmann et al. 2016)

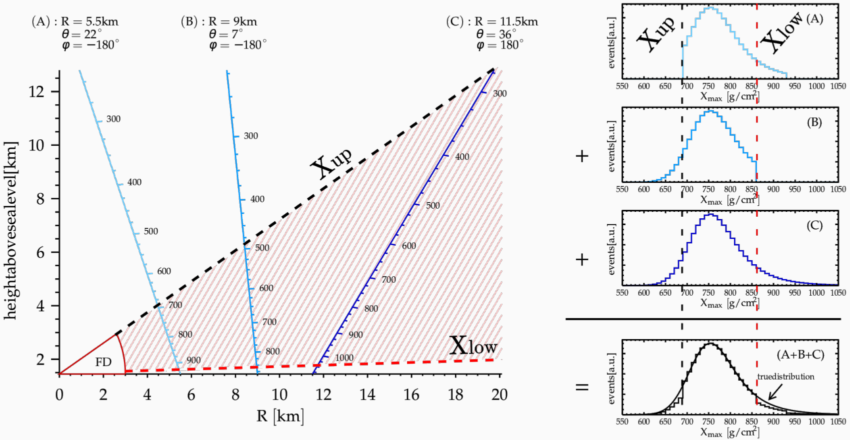

(A. Aab et al. 2014)

X_{max} must be in FoV to pass quality cuts

Geometry determines which X_{max} values will be measured.

Fiducial FoV Cuts

Distributions biased when
$X_{\text{low}}^{\text{fid}} < X_{low}$ or FoV top $X_{\text{up}}^{\text{fid}} > X_{up}$

(A. Aab et al. 2014)

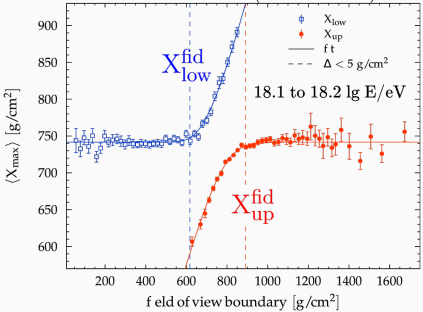

(A. Aab et al. 2014)

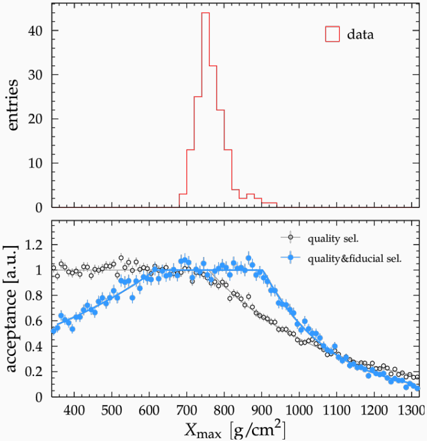

Fiducial cut flattens X_{max} acceptance for the majority of selected events.
Events with non-flat acceptance up-weighted via acceptance parameterization

Selection and detector X_{max} acceptance On/Off-plane

X_{max} acceptance of on- and off-plane probed with Sibyll-2.3c CONEX showers (p, Fe) with the profile shifted so that $X_{max} \in [300, 1500]$ g/cm^2 is sampled evenly

- Detector simulations account for time dependent state of the detector
- On- and off-regions corrected separately
  $\rightarrow$ weighting method from 2014 PRD employed
  (A. Aab et al. 2014)
- 1.4 % events in data have less than full acceptance

Detector and selection acceptance agree well within uncertainties

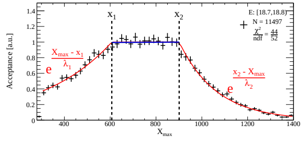

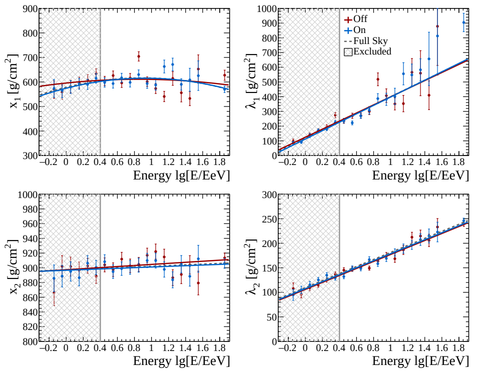

X_{max} Resolution and Systematic Uncertainties

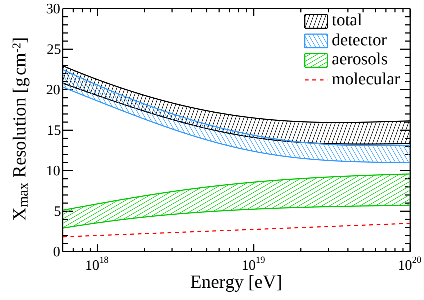

X_{max} Resolution

Effects from the atmosphere and the detector are combined into the X_{max} resolution to correct the X_{max} distributions.

Systematic uncertainties from the atmosphere, FD calibration reconstruction and detector are summed for systematic error of the moments

(A. Aab et al. 2014)

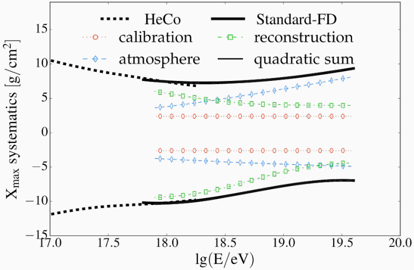

Systematic uncertainty of X_{max} scale

X_{max} Reconstruction bias and resolution On/Off-plane

X_{max} rec. bias and resolution on- and off-plane probed with 4-component (H, He, N, Fe) Sibyll-2.3c CONEX showers

- Detector simulations account for time dependent state of the detector
- Components reweighed to (Bellido 2018) mass fractions by energy
- Event-by-event comparison of reconstructed X_{max} to MC truth
- On- and off-regions each corrected by their energy parameterization

Reconstruction bias and resolution agree well within uncertainties

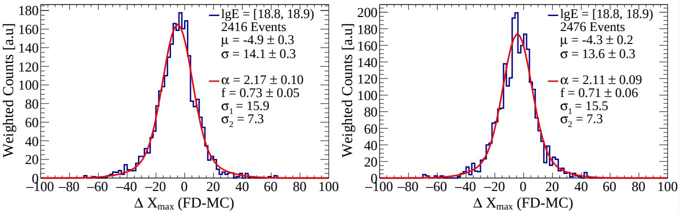

On plane

Off plane

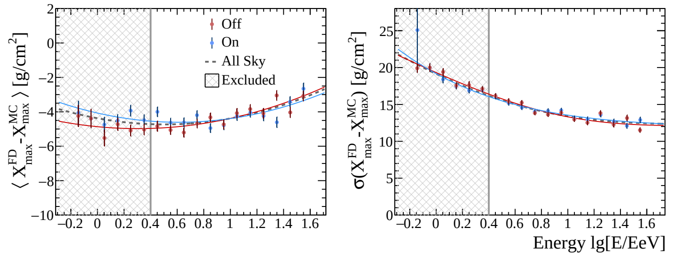

Systematic Error Summary from (A. Aab et al. 2014)

Error Source	Ref.	$\langle X_{max} \rangle$ Error [g/cm^2] 18.4 lg(E/eV)	19.6 lg(E/eV)	Applies to comparative analysis?
Detector Calibration		$\sim \pm 3$		
SD-FD Timing Offset		$\lesssim \pm 2$		no: applies to all events
Pixel Calibration		$\lesssim \pm 1$		**yes: Eye-to-Eye differences**
Telescope Alignment		$\lesssim \pm 1$		**yes: Eye-to-Eye differences**
Reconstruction		$^{+4.3}_{-8.2}$	$^{+4.0}_{-4.2}$	
Reconstruction Bias		0		**yes: sky region differences**
Profile Fit Function		± 4		no: applies to all events
Lateral Width Correction		$^{+1.6}_{-7.1}$	$^{+0.1}_{-1.3}$	no: On/Off Plane geometric similarity
Atmosphere		$\lesssim ^{+4.6}_{-3.8}$	$\lesssim ^{+7.5}_{-4.7}$	
Fluorescence yield		± 0.4		no: applies to all events
Multiple Scattering		$\lesssim \pm 2$		no: On/Off Plane geometric similarity
VAOD Systematics		± 1.6	± 2	**yes: seasonal variation of VAOD**
VAOD Uniformity		± 2.8	± 3.7	
VAOD Normalization		$+2.5$	$+6.5$	
Other		$\lesssim ^{+2.5}_{-1.5}$		
X_{max} Acceptance		$\lesssim \pm 1.5$		**yes: sky region differences**
Invisible energy		$\lesssim +1.2$		no: applies to all events
Total from dedicated studies		$\lesssim ^{+2.60}_{-2.18}$	$\lesssim ^{+3.80}_{-2.77}$	**see below**

Systematic Error Summary

Source	Uncertainty [g/cm²] $\Delta\langle X_{max}\rangle$	$\Delta\sigma(X_{max})$
X_{max} Acceptance	**$^{+1.14}_{-0.71}$**	**$^{+2.37}_{-1.61}$**
Rec. Bias	**±0.36**	**±0.01**
Rec. Resolution	**0**	**$^{+1.78}_{-0.24}$**
Seasonal variation	$^{+1.00}_{-1.53}$	$^{+1.19}_{-1.23}$
Instrumentation	±1.41	±1.41
Sum in Quadrature	$^{+2.10}_{-2.23}$	$^{+3.49}_{-2.48}$

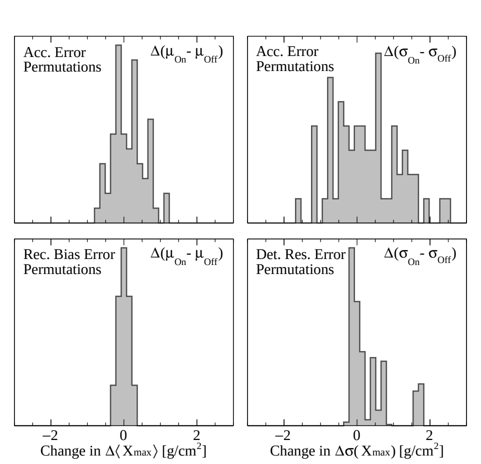

Changes to the magnitude of the end result using a permutation of all parameterization errors

Systematic Error Summary

Source	Uncertainty [g/cm^2] $\Delta\langle X_{max}\rangle$	$\Delta\sigma(X_{max})$
X_{max} Acceptance	$^{+1.14}_{-0.71}$	$^{+2.37}_{-1.61}$
Rec. Bias	± 0.36	± 0.01
Rec. Resolution	0	$^{+1.78}_{-0.24}$
Seasonal variation	$^{+1.00}_{-1.53}$	$^{+1.19}_{-1.23}$
Instrumentation	± 1.41	± 1.41
Sum in Quadrature	$^{+2.10}_{-2.23}$	$^{+3.49}_{-2.48}$

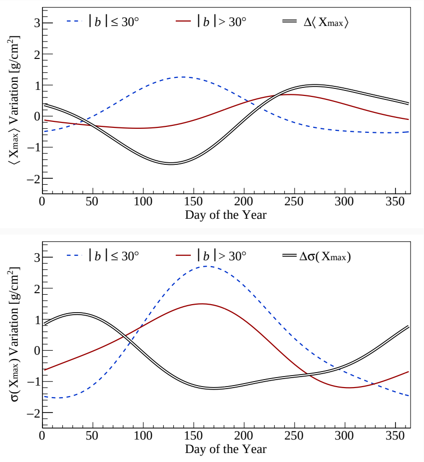

Observed variation of the first two moments of the on- and off-plane X_{max} distributions weighted by exposure.

Systematic Error Summary

Source	Uncertainty $[g/cm^2]$ $\Delta\langle X_{max}\rangle$	$\Delta\sigma(X_{max})$
X_{max} Acceptance	$^{+1.14}_{-0.71}$	$^{+2.37}_{-1.61}$
Rec. Bias	± 0.36	± 0.01
Rec. Resolution	0	$^{+1.78}_{-0.24}$
Seasonal variation	$^{+1.00}_{-1.53}$	$^{+1.19}_{-1.23}$
Instrumentation	± 1.41	± 1.41
Sum in Quadrature	$^{+2.10}_{-2.23}$	$^{+3.49}_{-2.48}$

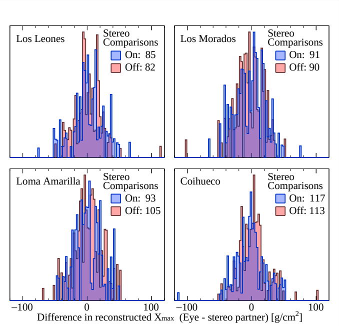

Site	events	Off − On plane bias $\langle X_{max}\rangle$	$\sigma(X_{max})$
LL	167	-0.8 ± 3.7	-3.2 ± 2.5
LM	181	-1.1 ± 3.7	-1.0 ± 2.5
LA	198	-0.1 ± 3.2	$+0.7 \pm 2.2$
CO	230	**3.0 ± 3.1**	-2.5 ± 2.1

Comparisons of on- and off-plane X_{max} reconstructions between FD-sites using stereo events.

Energy normalized FidFoV X_{max} on- and off-plane plotted separately vs time.

- Points are sets of 10 events
- Lines are cumulative means
- Solid fill is the running average over surrounding 40 events

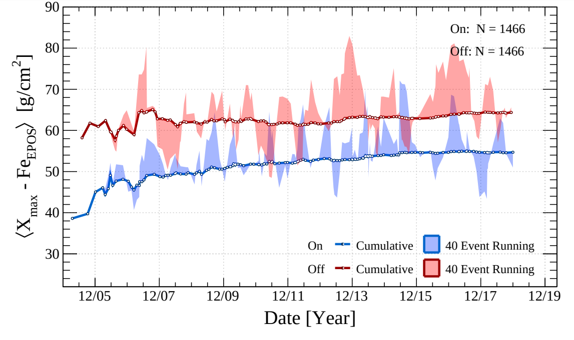

Both On and Off separately display a similar trend to those seen in other studies

No apparent affect on result.

Backup - Test Statistic

$$z_i = X_{max}^{norm} = X_{\max i} - EPOS_{Fe}(E_i)$$

Anderson-Darling 2 Sample Homogeneity Test

$$TS_{\mathrm{AD}} = \frac{n-1}{n^2} \sum_{i=1}^{2} \left[\frac{1}{n_i} \sum_{j=1}^{L} h_j \frac{(nF_{ij} - n_i H_j)^2}{H_j (n - H_j) - \frac{1}{4} n h_j} \right]$$

Modification to add sensitivity to distribution ordering

$$TS = \begin{cases} TS_{\mathrm{AD}} & : \langle X_{max}^{norm} \rangle^{on} < \langle X_{max}^{norm} \rangle^{off} \\ -3 & : else \end{cases},$$

n size of pooled sample

n_i size of sample i

z_j the value of the j^{th} event in the combined data set ordered from smallest value to largest

h_j is number of events in the pooled sample with a value equal to z_j

H_j is number of events in the pooled sample with a value less than $z_j + \frac{1}{2} h_j$

F_{ij} is number of events in the i^{th} sample with a value less than $z_j + \frac{1}{2} h_j$

Measuring X_{max}: geometry reconstruction

Pixel Trace	→	**Shower Plane**
		↓
Pixel/SD Timing	→	**Hybrid Geometry**
		⇣
Aperture Photons + Atmosphere	⇢	Light at Shower
		⇣
Gaisser-Hillas	⇢	Profile and X_{max} Dist

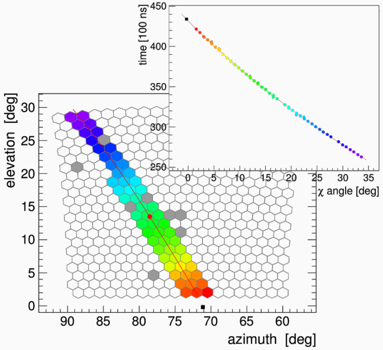

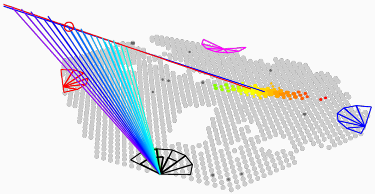

Measuring X_{max}: Shower Profile Reconstruction